MATERIALE PLASTICE
https://revmaterialeplastice.ro
https://doi.org/10.37358/Mat.Plast.1964

Influence of Biphasic Calcium Phosphate Incorporation Into Alginate Matrices

ALEXANDRU PAHOMI[1,2*], IONELA-AMALIA BRADU[1,5], DORIAN-GABRIEL NEIDONI[4], GHEORGHE ILIA[2,3]

[1]West University of Timisoara, Research Centre for Thermal Analysis in Environmental Problems, J. H. Pestalozzi Str. 16A, 300115, Timisoara, Romania
[2]West University of Timisoara, Faculty of Chemistry, Biology, Geography, J. H. Pestalozzi Str. 16A, 300115, Timisoara, Romania
[3]"Coriolan Dragulescu" Institute of Chemistry, 24 Mihai Viteazu Blvd., 300224, Timisoara, Romania
[4]National Research and Development Institute for Industrial Ecology- ECOIND, Timisoara Subsidiary, 115 Bujorilor Str., 300431, Timisoara, Romania
[5]West University of Timisoara, ICAM–Advanced Environmental Research Institute, 4 Oituz Str., 300233, Timisoara, Romania

***Abstract**: Biphasic calcium phosphate (BCP), containing β-tricalcium phosphate and hydroxyapatite, was synthesized by co-precipitation method to obtain a biomimetic artificial bone-like composite using calcium nitrate tetrahydrate [$Ca(NO_3)\cdot 4H_2O$] as calcium precursor and ammonium dihydrogen phosphate ($NH_4H_2PO_4$) as phosphorous precursor, maintaining Ca/P ratio of 1.67. The synthesized biphasic calcium phosphate mixture was dispersed in a sodium alginate (Alg) matrix dissolved in distilled water and lyophilized. The chemical structure, possible interactions between components and morphology of the obtained powder and scaffolds were studied through Fourier transform infrared (FT-IR) spectroscopy, X-ray diffraction (XRD) thermogravimetric analysis (TGA) and scanning electron microscopy (SEM) in order to observe the interactions between BCP and the polymer. The particle size of the powder was also analyzed using the dynamic light scattering (DLS) analysis. Calcined powder had a particle size of 1.8 µm. In addition to the low crystalline hydroxyapatite (HA), as the main phase in the dried samples, β-tricalcium phosphate (β-TCP) was formed after the thermal treatment of 1000˚C as shown by XRD and FT-IR. The obtained composite material presented* a *highly porous microstructure with interconnected layers where the BCP particles were well dispersed. The micro-structure of the scaffolds was influenced with the change in pore dimensions and rearrangement of the layers due to the incorporation of the BCP particles and by the treatment of the scaffolds with* $CaCl_2$.

***Keywords:** hydroxyapatite, chitosan, sodium alginate, bonelike composite, scaffold*

1. Introduction

Tissue engineering (TE) has become a promising technique for repairing damaged tissues and it requires suitable biocompatible materials that can be used as scaffolds for the seeding with cells for the growth of new tissue.

Research suggests that nano-structured composites using biodegradable polymers and bioactive ceramics such as hydroxyapatite (HA), and $Ca_5(PO_4)_3OH$, possess the ability to simulate the surface and chemical properties of bone [1, 2].

Hydroxyapatite, which constitutes a major component of the bone, consisting 70% by weight of the human bone, has become a very studied material with great implications in the areas of biomaterials and tissue engineering, especially in bone regeneration due to its high bioactivity and osteo-conductive properties [3, 4]. It also exhibits proprieties that find applications as a drug carrier [5], as a filler for bone repairing and replacement [6] and as a coating for prosthetic implants [7]. Hydroxyapatite is a natural occurring mineral that can be synthesized using different methods, such as: wet chemical precipitation [8], sol-gel method [9], solid-state reactions [10] and high-temperature methods as combustion or pyrolysis [11, 12].

email: alexandru.pahomi@e-uvt.ro

Taking into consideration all the properties required in scaffolds in order to have applications in bone regeneration, such as: biocompatibility, cell proliferation and growth, biodegradability, mechanical integrity and flexible processing methods, the optimum system seems to be polymer matrix composites containing hydroxyapatite [2]. Due to the use of the scaffolds in the medical field, it is important to take into consideration the effect of sterilization on the characteristics of the material. It was reported that exposure to radiation alters the physical and chemical properties of the polymer. Depending on the method of sterilization used, the polymer can be degraded, undergo crosslinking, or change charge, thus affecting the required properties for bone regeneration. Also, the phase composition of hydroxyapatite can change due to sterilization. As reported in a recent study by Predoi et al., exposure to gamma irradiation induced the transformation of hydroxyapatite in β-TCP [13], this kind of irradiation being one of the most used in medical applications [14, 15]. Hydroxyapatite can also produce intercalated structures with polymers [16, 17]. Tsiourvas et al. reported the development of porous composite scaffolds consisting of chitosan or N-acetylated chitosan and HA at high content (75% w/w) successfully obtaining complex three-dimensional shapes [18]. Usually, β-TCP is present beside hydroxyapatite, and it is one of the most known calcium phosphates. It is more biodegradable than hydroxyapatite and provides a source of calcium and phosphorus for bone formation [19]. During degradation it stimulates the osteoblastic function and promotion of bone formation [20, 21]. A biphasic calcium phosphate mixture can be obtained when calcium-deficient apatite is thermally treated at or above 700^{o}C and the calcium deficiency can be influenced by the synthesis method used, the *p*H of the reaction or temperature. If the calcium deficiency of the apatite is low, the percentage of hydroxyapatite in the biphasic mixture is higher. By adjusting the HA/ β-TCP ratios in the BCP mixture, it's properties and biological activity can be tailored to achieve a specific application in tissue engineering [18].

Sodium alginate (Alg) meet the properties required to be used as matrices for scaffolds with applications in tissue engineering. Sodium alginate (Alg) is a naturally occurring polysaccharide polymer derived from brown sea algae. In the presence of a low concentration of divalent cations it will form a stable hydrogel as a result of the ionic interaction between carboxylic groups in the alginate structure chain and the divalent cations. Alginate exhibit hydrophilic features and tend to be degradable under physiological environments. It presents biocompatibility and low toxicity, making it suitable for biological applications [22]. Various methods for preparation of hydroxyapatite/polymer composites were described in literature such as freeze-drying [23], thermally induced phase separation [24], melt extrusion [23], electrospinning method [25], layer-by-layer technique [26] or uniaxial hot-pressing [27].

In this study, we focused on using the co-precipitation method to obtain biphasic calcium phosphate. Because of the synthesis method used, the powder obtained contained amorphous hydroxyapatite that suffered a phase transformation after the thermal treatment of the samples. By analyzing the results, an indebt characterization of the samples is presented with the aim to explain the properties that are affected by the presence of BCP in the alginate matrix.

The study led to the fabrication of highly porous scaffolds containing biphasic calcium phosphates. The particularity of this type of scaffolds is given by a higher pore dimension compared to similar scaffolds. The pore dimension and the interconnectivity of the layers makes them suitable for usage in bone tissue regeneration, with an emphasis on the osteogenic effect. The addition of the biphasic calcium phosphate mixture, containing hydroxyapatite and β-TCP, can give enhanced properties to the final materials.

2. Materials and methods

2.1. Materials

Materials used for synthesis of biphasic calcium phosphate mixture were $Ca(NO_3)\cdot 4H_2O$ (KEBO Lab), $NH_4H_2PO_4$ (Sigma Aldrich), and NH_3 aq. (Sigma Aldrich). For the polymer matrix sodium alginate (VWR, Prolabo) was used. The preparation method implied the treatment with $CaCl_2$ (Sigma Aldrich) of the obtained scaffolds. All reagents were of analytical grade and deionized (DI) water was used in all experiments.

2.2. Synthesis of biphasic calcium phosphate mixture

To synthesize HA, the method described by Ghosh and Sarkar was used by dissolving $Ca(NO_3)\cdot 4H_2O$ in distilled water and adding in the phosphorous precursor solution dropwise under stirring, maintaining the Ca/P ratio at 1.67. Beforehand, the *p*H of each solution was adjusted to 10. The synthesis protocol used was based on the next reaction:

$$10\,Ca(NO_3)_2 + 6\,NH_4H_2PO_4 + 14\,NH_4OH \longrightarrow Ca_{10}(PO_4)_6(OH)_2 + 20\,NH_4NO_3 + 12\,H_2O$$

The *p*H of the mixture was adjusted at 10 and stirred for 2h, while checking the *p*H of the mixture and correcting it if needed. After the first 2h, the mixture was left to age for 24h.

After aging, the slurry mixture was filtered under vacuum and dried at 120°C. To obtain a crystalline form, the resulted powder was calcined at 1000°C for 12h [28].

2.3. Synthesis of alginate/BCP scaffolds

The preparation method of the scaffolds was adapted from the protocols used by Tsiourvas et al. and Li et al. [18, 29]. Alg was dissolved in deionized (DI) water until a homogenous 1 wt.% sodium alginate solution was obtained.

After the complete dissolving of the polymer, the solution was split into two parts. One part of the polymer solution was used to obtain reference scaffolds. Into the other part of the polymer solution, calcined BCP was dispersed at a weight ratio of 1:1 (HA/Alg), stirred at room temperature for 6h, and sonicated for 30 min. After the sonication, the resulting solution was cast in 24-well cell culture plates, froze, and lyophilized using a ScanVac Coolsafe 110-4 freeze dryer until complete water evaporation. The reference scaffolds, containing only sodium alginate, were subjected to the same preparation method, without BCP.

The scaffolds with BCP were defined as Alg-BCP and the reference scaffolds without BCP were defined as Alg.

Some scaffolds were analyzed as obtained and some were treated to observe how the treatment affect certain properties of the obtained scaffolds. The scaffolds containing sodium alginate were cross-linked with Ca^{2+} ions by immersing the scaffolds in a 5 % (w/v) $CaCl_2$ solution for 12h, washed thoroughly with deionized water, and lyophilized.

2.4. Characterization

FT-IR analysis was conducted using a Perkin-Elmer Spotlight 400+ Spectrum 100 FT-IR spectrometer. The spectra were recorded over a range of 4000-500 cm^{-1} at 2 cm^{-1} resolution. XRD analysis was performed using a PANalytical diffractometer, with Cu-Kα radiations ($\lambda = 0.15406$ nm) in a 2θ range from 10 to 90°. Thermal properties were determined using a Mettler Toledo TGA/DSC 1 analyzer from 30 to 900°C at a heating rate of 10°C · min^{-1} under nitrogen atmosphere (50 mL/min). The morphology of the scaffolds was observed with a Hitachi S4800 field emission scanning electron microscope at an accelerating voltage of 1 kV and a Cressington 208HR used for sputtering. The average particle size of the powders was measured using a Malvern Zetasizer Nano ZS with a He-Ne laser (633 nm) as a source of the incident light.

3. Results and discussions

3.1. Characterization of synthesized BCP

3.1a. FT- IR spectroscopy

Figure 1 shows the FT-IR spectra of biphasic calcium phosphate mixture after the filtration under vacuum and drying at 120°C. The IR bands at 960 cm^{-1}, 1025 cm^{-1}, and 1090 cm^{-1} are attributable, respectively, to the symmetric and asymmetric stretching of PO_4^{3-} groups of the hydroxyapatite structure. The bands at 3573 cm^{-1} and 633 cm^{-1} are attributable to the symmetric stretching of HO^-,

respectively the lattice HO^-. The broad band around 3400 cm^{-1} and the band around 1636 cm^{-1} correspond to the water molecules adsorbed on the powder surface. Besides, the two bands located at 870 and 1454 cm^{-1} were assigned to the CO_3^{2-} groups due to CO_2 adsorption from atmosphere during synthesis. At 1332 and 824 cm^{-1}, the bands observed correspond to NO_3^- as synthesis residue [30, 31].

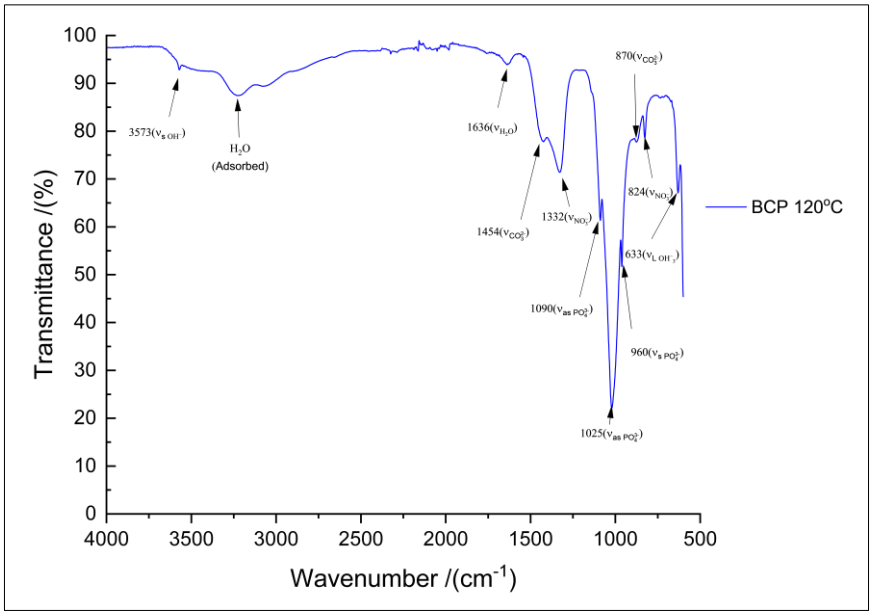

Figure 1. FT-IR spectra of BCP powder dried at 120°C

After thermally treating the sample at 1000°C for 12 h it can be observed (Figure 2) that the bands corresponding to CO_3^{2-} and NO_3^- disappear completely, alongside with the bands attributed to water adsorption. It can be observed that a sharp band at 3570 cm^{-1} was maintained after the thermal treatment, a band belonging to the symmetric stretching of HO^-. The band at 633 cm^{-1} band can be observed. Beside the band characteristic for hydroxyapatite, a band at 970 cm^{-1} can be distinguished. It could be suggested that a second phase could be present in traces in the calcined powder [32].

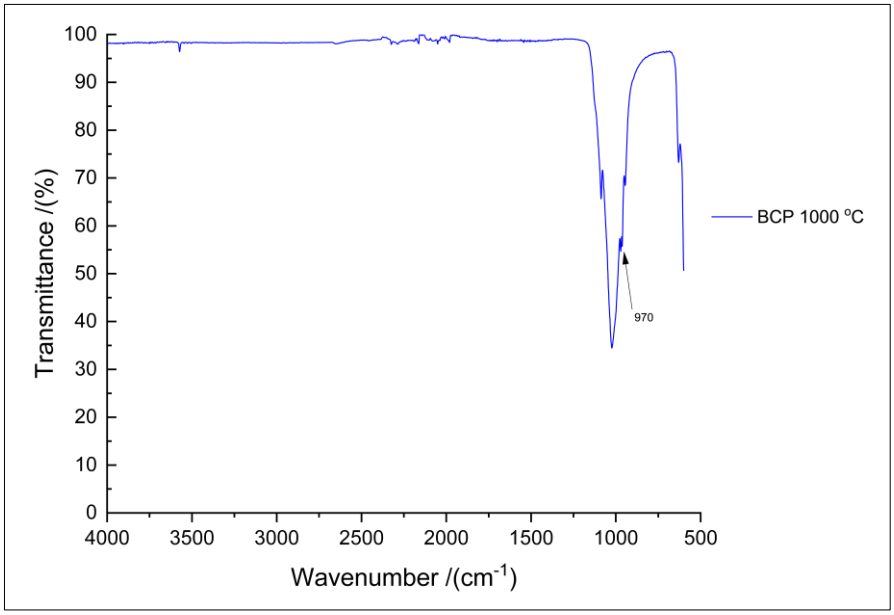

Figure 2. FT-IR spectra of BCP powder calcined at 1000°C

3.1b. Thermal analysis

Figure 3 illustrates the results of thermogravimetric analysis (TGA) and differential thermal analysis (DTA) for the precursor precipitated at *p*H= 10 and dried at 120°C.

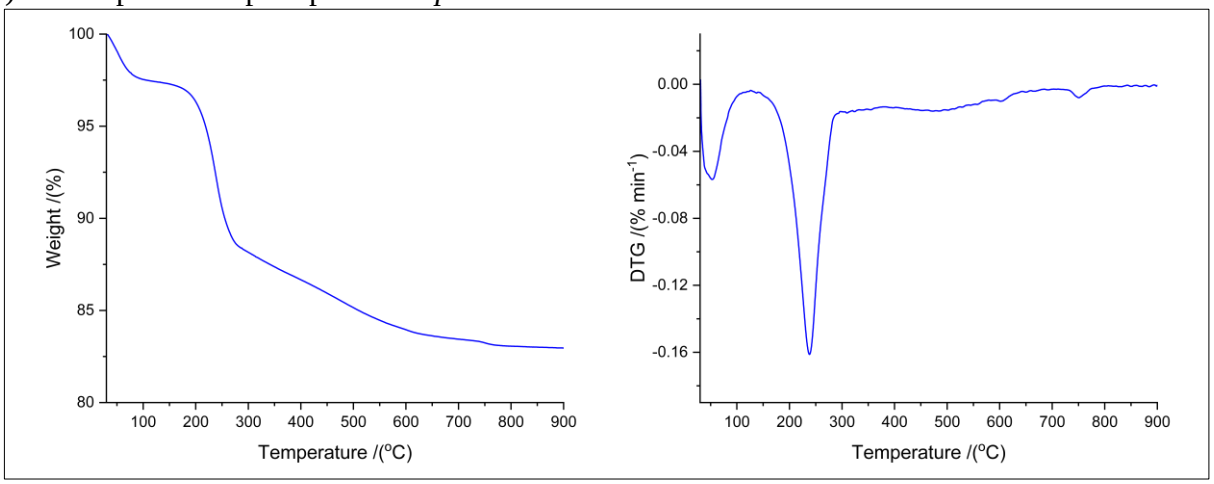

Figure 3. TGA and DTA curves for BCP dried at 120°C

The weight loss of the sample is taking place in three stages. The sample has an endothermic peak in the range of 30-100°C with a 2% weight loss corresponding to the loss of physically absorbed water molecules. A secondary endothermic peak at ~240°C is shown by the removal of crystallized water, characterized by an 8% weight loss.

A continuous weight loss of 4% mass till around 750°C is observed. Above this temperature a sharp endothermic peak appears at 770°C accompanied by a 1% weight loss, attributed to the decomposition of non-stoichiometric hydroxyapatite to β–TCP and H_2O [33, 34].

3.1c. X-ray diffraction

The phase of the dried precursor at 120 and 1000°C has been studied using XRD (Figure 4). The pattern of the dried sample shows broad peaks and the phase identified in the sample was low crystalline hydroxyapatite. X-ray diffractogram of the sample treated at 1000°C shows sharp peaks which indicates the increase of the sample crystallinity. The phases present in the sample were identified and are summarized in Table 1. Two phases were identified in the diffraction patterns and the composition of the two samples indicates to be a mixture of HA and β–TCP, containing 45% HA and 55% β–TCP.

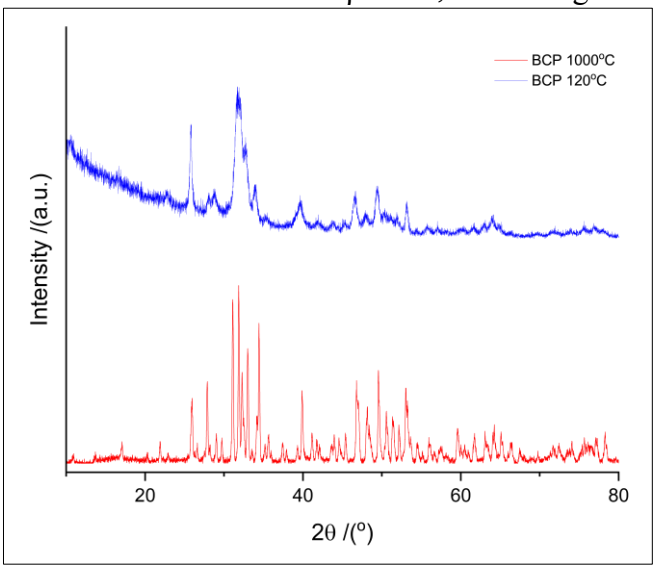

Figure 4. Powder X-ray diffraction pattern of the sample dried at 120°C (blue) and calcined at 1000°C (red)

Table 1. Phases and mass fraction of the synthesized samples thermally treated at 1000°C

Sample	Phase mass fraction (%)	
	HA	β–TCP
BCP 1000°C	45.04	54.96

3.1d. DLS analysis

A 15 mL suspension of 10 mg of each sample dried at 120°C and thermally treated at 1000°C was prepared in deionized water by ultrasonication followed by centrifugation. From that 2 mL of the suspension was taken in a cuvette and used for the measurement of particle size. Each sample was measured three times at a scattering angle of 173°.

The PDI (polydispersity index) read by the instrument for the samples dried at 120°C shows a mid-range polydispersity. After the thermal treatment of the samples, PDI increases showing a polydisperse system and indicating that more agglomerates are forming after the thermal treatment. Since the PDI ranging from 0.1-0.5 is suitable for measurements and has a good quality of the colloidal suspensions, the results in Table 2 indicate that the samples can be well dispersed in water and form a stable and uniform aqueous suspension [33, 34].

The average particle size of the samples dried at 120°C ranges was 2.1 µm. After the thermal treatment, the sample showed a decrease of the average particle size almost by 15% of the initial size as shown in Table 2.

Table 2. DLS analysis results of sample dried at 120°C and thermally treated at 1000°C

Sample	Z-Ave (d.µm)		PDI	
	120°C	1000°C	HA	120°C
BCP	2.1	1.8	BCP	2.1

3.1e. Scanning electron microscopy

Figure 5 shows the SEM images of the dried precursor and the powder obtained after thermal treatment at 1000°C for 12 h. The dried powder at 120°C appear to be highly agglomerated, with agglomerates up to 7-8 µm and the smaller particles ranging between 2.5-4 µm (Figure 5a). The powder obtained after the thermal treatment at 1000°C for 12 h exhibits the morphology of sintered platelets as shown in Figure 5b. It appears that fine particles (400-800 nm) have been sintered during the thermal treatment, alongside particles that have around 4-5 µm.

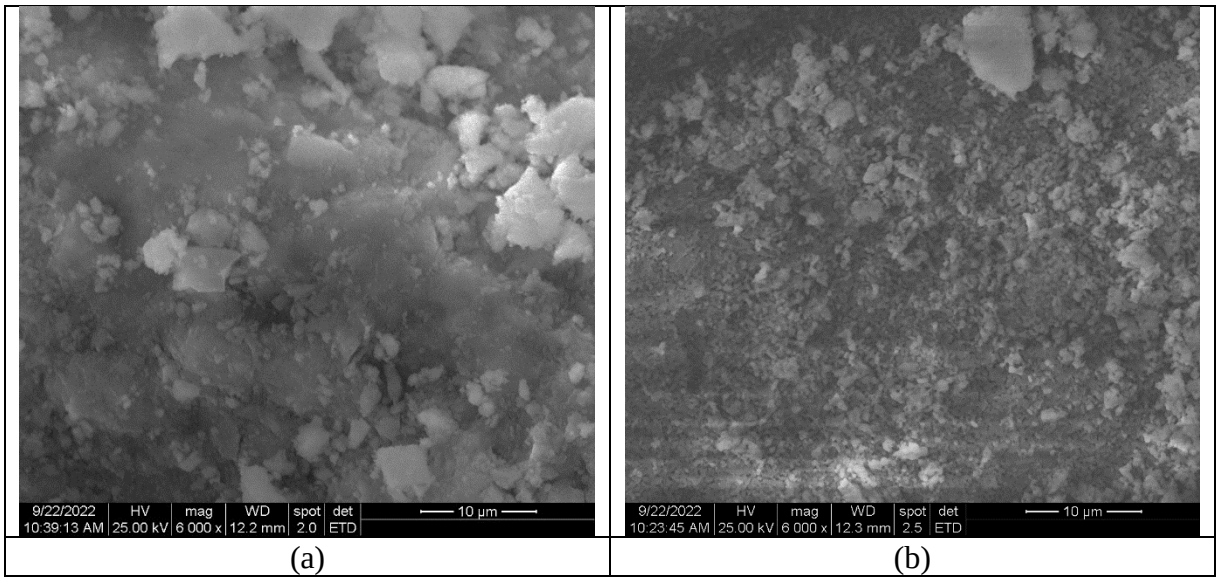

(a) (b)

Figure 5. SEM images of sample dried at 120°C (a) and sample thermally treated at 1000°C (b)

The data observed from the XRD correlates with the results observed from FT- IR spectroscopy and thermal analysis and, as confirmed by the XRD analysis, biphasic calcium phosphate resulted after the thermal treatment of the samples

3.2. Characterization of synthesized scaffolds

The obtained scaffolds after dispersion of the calcined BCP particles were characterized using FT-IR spectroscopy, thermal analysis, and scanning electron microscopy.

3.2a. FT- IR spectroscopy

The spectrum for the sodium alginate powder used in scaffold preparation is presented in Figure 6 and showed a large absorption band in the range of 3600 - 3000 cm^{-1} due to the stretching vibration band of OH group and the CH vibration bands at 2941 cm^{-1}. The intense bands observed at 1593 cm^{-1} and 1410 cm^{-1} were correlated to the asymmetric and symmetric stretching of C=O in the $-COO^-$ groups indicating the presence of the carboxylic acid group in the alginate. The bands measured at 1068 and 1033 cm^{-1} may be attributed to C-O stretching vibrations and C-C stretching vibrations of pyranose rings. Moreover, the stretching vibration bands observed around 950-810 cm^{-1} are specific to the guluronic and mannuronic acids present in the structure alginate structure.

The FT-IR spectra of scaffolds tend to be consistent with each other and the specific bands of the components are overlapping, as seen in Figure 7. The treatment with $CaCl_2$ was applied to avoid the dissolution of the alginate scaffolds in water and because of to the well-known crosslinking effect of bivalent cations on the alginate chain. When exposed to multivalent cations, the alginate chains begin to interact with the ions that form crosslinks with other nearby chains. It is indicated in literature that the interactions of Ca^{2+} ions are located at the $-COO^-$ groups and can be observed in the FT-IR spectra by the shift to lower wavenumbers of the asymmetric and symmetric stretching of C=O [35, 36]. In the spectra of the treated scaffolds the bands from 1593 and 1410 cm^{-1} shift to 1570 and 1400 cm^{-1}, respectively. Also, the shoulder at 1068 cm^{-1} relating to the C-O stretching strengthens and can be distinguished in the spectra treated samples and is an indication of crosslinking [37].

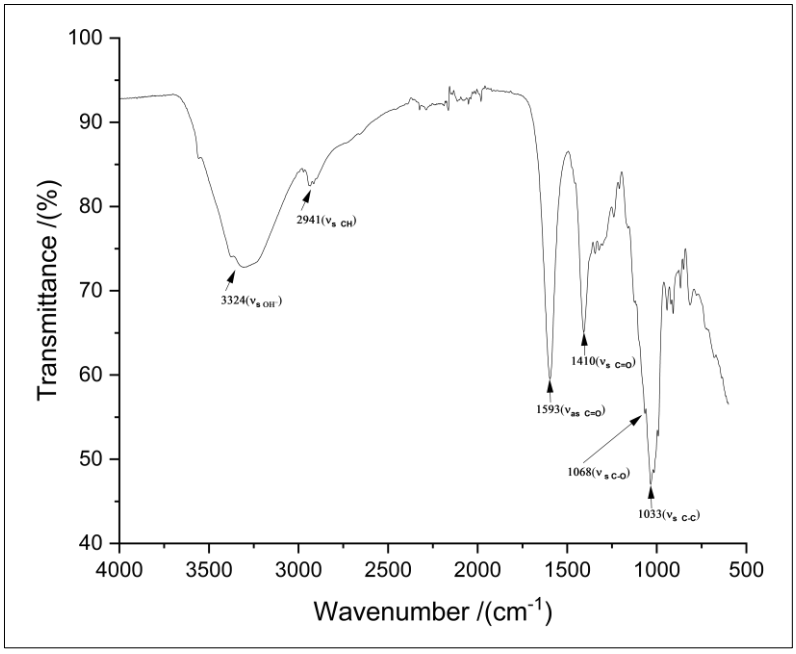

Figure 6. FT-IR spectrum of sodium alginate powder (VWR, Prolabo)

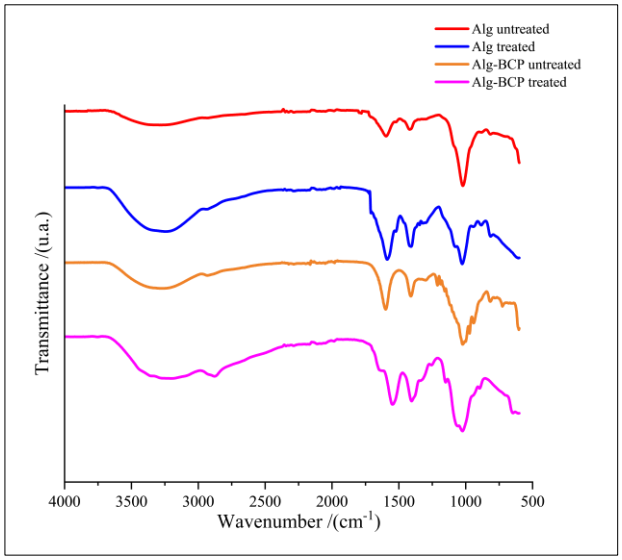

Figure 7. FT-IR spectra of alginate scaffold untreated (Alg untreated), alginate scaffold treated with $CaCl_2$ 5% (Alg treated), alginate scaffold containing BCP untreated (Alg-BCP untreated) and alginate scaffold containing BCP treated with $CaCl_2$ 5% (Alg-BCP treated)

3.2b. Thermal analysis

The results of thermogravimetric analysis (TGA) and differential thermal analysis (DTA) for the scaffolds are presented in Figure 8. Due to the high thermal stability of hydroxyapatite, the curves indicate the thermal behavior of the used polymers in powder and scaffold form. Sodium alginate depicts weight loss in three stages. The first stage appears in the range of 50-110^{o}C and is associated with the loss of physically absorbed water molecules and is characterized by an endothermic peak with a weight loss of 5%. The second stage takes place in the range of 180-300^{o}C and was associated with the exo-thermic decomposition of the alginate carbon chains with a weight loss of 38%. In case of Alg powder and Alg untreated, sodium carbonate (Na_2CO_3) is formed as an intermediate product that decomposes exothermically in the range of 600-850^{o}C [35]. The total weight loss of the thermal treatment was 81%. Treated scaffold and, also, Alg-BCP untreated did not show a third stage of de-composing in the range of 600-850^{o}C after the treatment with $CaCl_2$ or the dispersion of BCP in the matrix concluding that no Na_2CO_3 was formed after crosslinking with Ca^{2+} ions. DTA curves indicate that crosslinking with Ca^{+2} ions and addition of BCP did not significantly change the temperature of the degradation process. It can be noted that the second stage of degradation ends at a higher temperature (~350^{o}C) which can be considered an increase in the thermal stability of the scaffolds [35, 38].

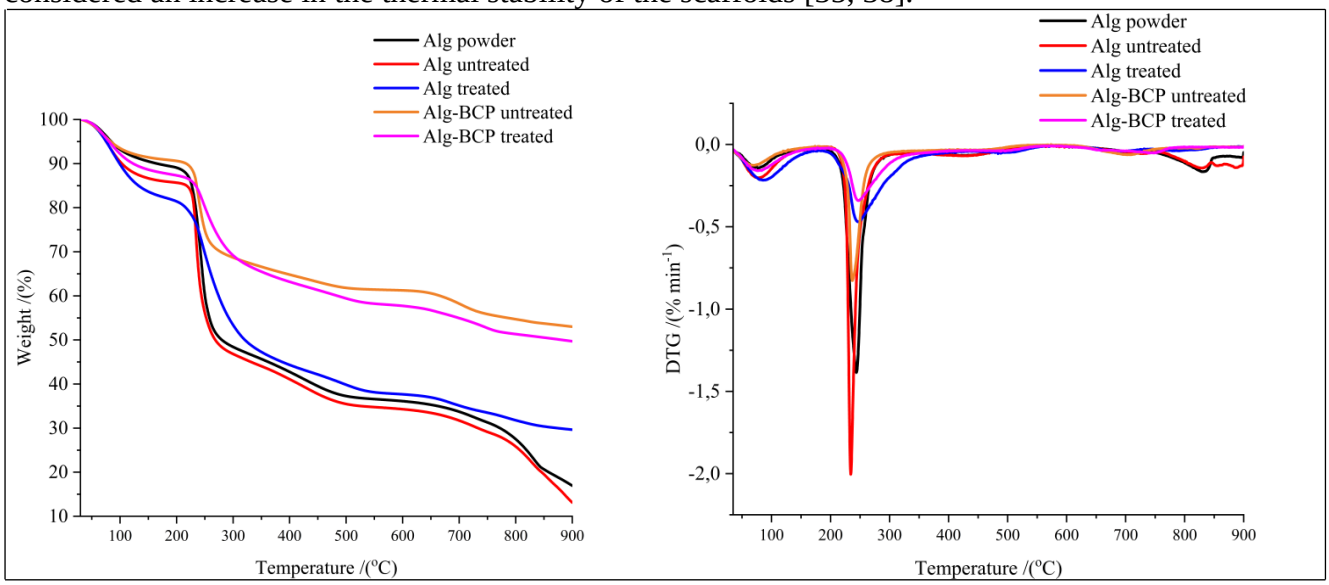

Figure 8. TGA and DTA curves of alginate powder (Alg powder), alginate scaffold untreated (Alg untreated), alginate scaffold treated with CaCl2 5% (Alg treated), alginate scaffold containing BCP untreated (Alg-BCP untreated) and alginate scaffold containing BCP treated with CaCl2 5% (Alg-BCP treated)3.2c. Scanning electron microscopy

The morphology of the scaffolds was investigated using field emission scanning electron microscopy. Prior to surface analysis, the samples were Pt/Pd coated with a layer thickness of approximately 7 nm through sputtering. As shown in the SEM images provided in Figure 9, the cross-sectional morphology of the alginate scaffolds showed that the three-dimensional porous microstructure was formed by the freeze-drying step, with the pores being the result of ice crystal formation. An open-pore microstructure with a high degree of interconnectivity was observed in all samples. A highly porous with interconnected layers microstructure can be observed in the alginate sample that isn't treated (Figure 9a). The alginate microstructure shows more individual pores with diameter of 100 to 200 μm after lyophilization. The crosslinking with $CaCl_2$ rearranges the microstructure and the distance between the interconnected layers increases from an average of 200 μm up to 500-700 μm (Figure 9b). With the addition of BCP in the scaffold composition the pore size decreases (Figure 9c) and it can be noticed that bigger hollow regions in the scaffold microstructure appear.

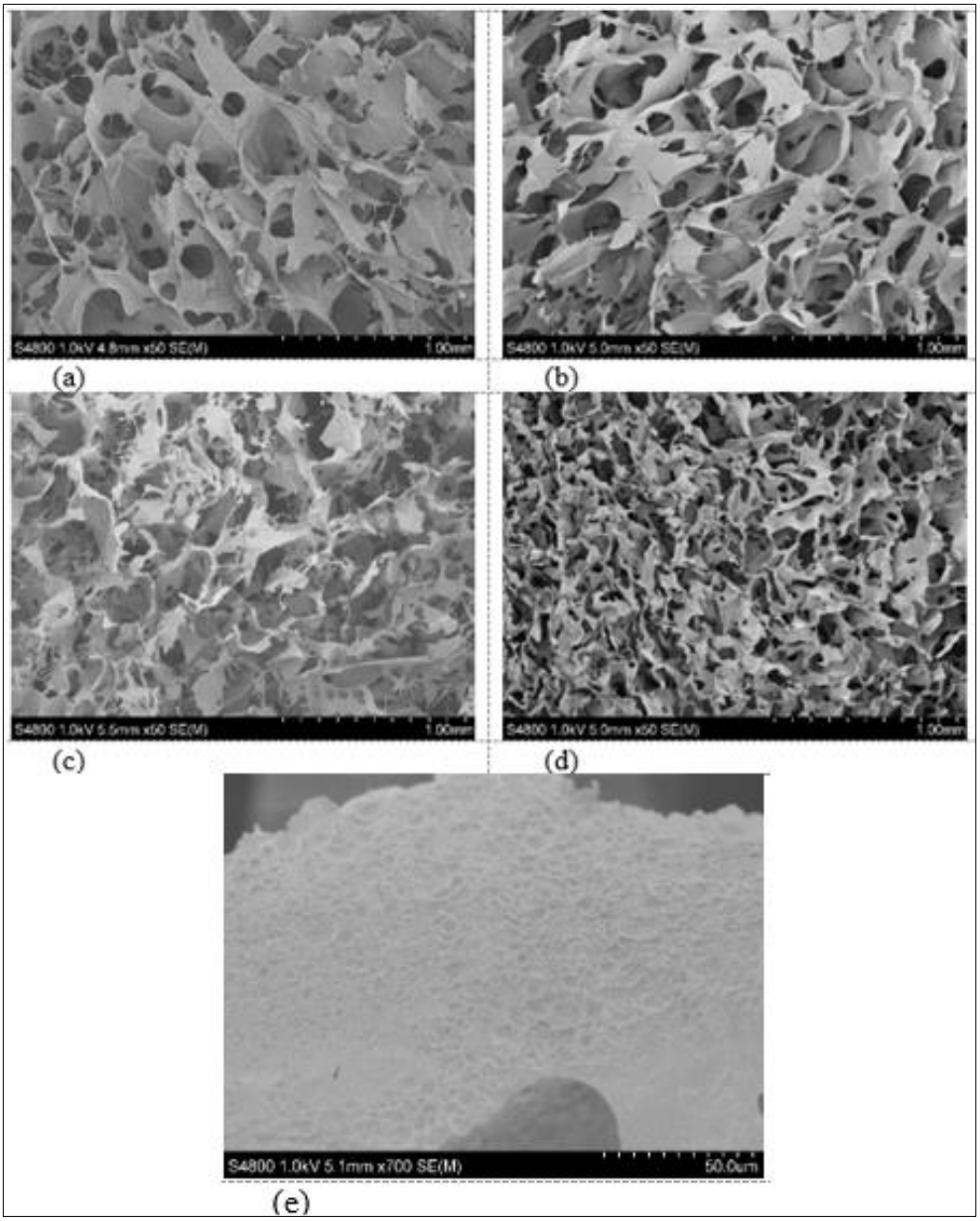

Figure 9. SEM images of alginate scaffold untreated (a), alginate scaffold treated (b), alginate scaffold containing BCP untreated (c), alginate scaffold containing BCP treated (d) all at x50 magnification and alginate scaffold containing BCP treated at x700 magnification (e)

A similar decrease in pore size was observed by Luo et al. by fabrication of porous hydroxyapatite–sodium alginate nanocomposite scaffolds and the decrease of pore size was attributed to hydroxyapatite acting as a ceramic filler [38]. After the treatment of the alginate scaffold containing BCP with $CaCl_2$ a more compact and layered microstructure is seen with an average distance between layers of around 100 µm (Figure 9d), with the BCP particles dispersed uniformly on the surface of the interconnected layers (Figure 9e).

As stated in other studies, cell adhesion, exchange between nutrients and bone regeneration are affected by the size of the pores and the connectivity between them. Investigations on the bone ingrowth derived by using porous materials showed an optimum pore size of 100-400 µm. Also, incorporation of a BCP mixture containing HA and β-TCP into a matrix with pores above 80 µm stimulates osteogenesis. High porosity of the scaffolds and a pore size between 100-350 µm make them usable for bone tissue engineering by facilitating cell binding and cell proliferation [32, 39-42].

Unabia et al. found that thermal treatment above 900^{o}C of hydroxyapatite precursors obtained by co-precipitation resulted in phase transition of hydroxyapatite to β-TCP and formation of a product containing biphasic calcium phosphates [43]. Others stated that co-precipitation method would form calcium deficient hydroxyapatite and at a thermal treatment between 900-1100^{o}C, β-TCP would form [44-46].

4. Conclusions

Using FT-IR spectroscopy and X-ray diffraction to characterize the powder after thermal treatment at 1000˚C concluded that the powders contained different phases and the resulted product was biphasic calcium phosphate consisting of hydroxyapatite and β-TCP due to the calcium deficient apatite, obtained initially. The X-ray diffraction confirmed that the co-precipitation method used led to synthesis of low crystalline hydroxyapatite and the thermal treatment gave a mixture of HA and β–TCP. The results were in accordance with the thermal analysis applied to the precursors precipitated at *p*H=10 and points to how the effect of the reagents used can influence the results.

Porous composite scaffolds were successfully obtained through freezing and lyophilization technique. The morphology of the microstructure indicated the formation of highly porous with inter-connected layers materials where the BCP mixture consisting of HA and β-TCP was well dispersed. The influence on the microstructure caused by the incorporation of the BCP mixture and the applied treatment was observed through the changes of pore dimensions and microstructure rearrangement. The addition of BCP decreases the pore size and bigger hollow regions in the scaffold microstructure appear. These modifications can be influenced by the water content of the initial polymer solution and freezing conditions of the samples applied prior of lyophilization. The FT-IR and thermal analysis indicated that the additional treatment of the polymer scaffolds and the incorporation of the BCP mixture into the matrices increase the stability and influence the structure of the samples.

Characterization of the microstructure indicated that the treated scaffolds containing BCP are suitable for bone tissue engineering because they can assure infiltration, binding and proliferation of cells.

References

1.MONDAL, S., PAL, U., DEY, A., Natural origin hydroxyapatite scaffold as potential bone tissue engineering substitute, *Ceram. Int.*, **42**, 2016, 18338-18346, https://doi.org/10.1016/j.ceramint.2016.08.165
2.ELTOM, A., ZHONG, G., MUHAMMAD, A., Scaffold Techniques and Designs in Tissue Engineering Functions and Purposes: A Review, *Adv. Mater. Sci. Eng.*, **2019**, 2019, https://doi.org/10.1155/2019/3429527
3.ROSETI, L., PARISI, V., PETRETTA, M., CAVALLO, C., DESANDO, G., BARTOLOTTI, I., GRIGOLO, B., Scaffolds for Bone Tissue Engineering: State of the art and new perspectives, *Mater. Sci. Eng. C*, **78**, 2017, 1246–1262, https://doi.org/10.1016/j.msec.2017.05.017

4. LEI, Y., XU, Z., KE, Q., YIN, W., CHEN, Y., ZHANG, C., GUO, Y., Strontium hydroxyapatite/chitosan nanohybrid scaffolds with enhanced osteoinductivity for bone tissue engineering, *Mater. Sci. Eng. C.*, **72**, 2016, 134–142, https://doi.org/10.1016/j.msec.2016.11.063
5. SUN, H., LIU, S., ZENG, X., MENG, X., ZHAO, L., WAN, Y., ZUO, G., Morphology effect of nano-hydroxyapatite as a drug carrier of methotrexate, *J. Mater. Sci. Mater. Med.*, **28**, 2017, 158, https://doi.org/10.1007/s10856-017-5978-4
6. RAUCCI, M.G., ALVAREZ-PEREZ, M., GIUGLIANO, D., ZEPPETELLI, S., AMBROSIO, L., Properties of carbon nanotube-dispersed Sr-hydroxyapatite injectable material for bone defects, *Regen. Biomater.*, **3**, 2016, 13–23, https://doi.org/10.1093/RB/RBV026
7. MISTRY, S., ROY, R., KUNDU, B., DATTA, S., KUMAR, M., CHANDA, A., KUNDU, D., Clinical outcome of hydroxyapatite coated, bioactive glass coated, and machined Ti_6Al_4V threaded dental implant in human jaws: A short-term comparative study, *Implant Dent.*, **25**, 2016, 252–260, https://doi.org/10.1097/ID.0000000000000376
8. ANWAR, A., KANWAL, Q., AKBAR, S., MUNAWAR, A., DURRANI, A., HASSAN FAROOQ, M., Synthesis and characterization of pure and nanosized hydroxyapatite bioceramics, *Nanotechnol. Rev.*, **6**, 2017, 149–157, https://doi.org/10.1515/ntrev-2016-0020
9. TÜRK, S., ALTINSOY, İ., ÇELEBI EFE, G., IPEK, M., ÖZACAR, M., BINDAL, C., Effect of Solution and Calcination Time on Sol-gel Synthesis of Hydroxyapatite, *J. Bionic Eng.*, **16**, 2019, 311–318, https://doi.org/10.1007/s42235-019-0026-3
10. INGOLE, V.H., HUSSEIN, K.H., KASHALE, A.A., GATTU, K.P., DHANAYAT, S.S., VINCHURKAR, A., CHANG, J.Y., GHULE, A.V., Invitro Bioactivity and Osteogenic Activity Study of Solid State Synthesized Nano-Hydroxyapatite using Recycled Eggshell Bio–waste, *Chemistry Select*, **1**, 2016, 3901–3908, https://doi.org/10.1002/slct.201601092
11. CANILLAS, M., RIVERO, R., GARCÍA-CARRODEGUAS, R., BARBA, F., RODRÍGUEZ, M.A., Processing of hydroxyapatite obtained by combustion synthesis, *Bol. la Soc. Esp. Ceram. y Vidr.*, **56**, 2017, 237–242, https://doi.org/10.1016/j.bsecv.2017.05.002
12. CHO, J.S., LEE, J.C., RHEE, S.H., Effect of precursor concentration and spray pyrolysis temperature upon hydroxyapatite particle size and density, *J. Biomed. Mater. Res. - Part B Appl. Biomater.*, **104**, 2016, 422–430, https://doi.org/10.1002/jbm.b.33406
13. PREDOI, D., CIOBANU, C.S., ICONARU, S.L., PREDOI, S.A., CHIFIRIUC, M.C., RAAEN, S., BADEA, M.L., ROKOSZ, K., Impact of Gamma Irradiation on the Properties of Magnesium-Doped Hydroxyapatite in Chitosan Matrix, *Materials (Basel)*, **15**, 2022, 5372, https://doi.org/10.3390/ma15155372
14. FARNO, M., LAMARCHE, C., TENAILLEAU, C., CAVALIÉ, S., DUPLOYER, B., CUSSAC, D., PARINI, A., SALLERIN, B., GIROD FULLANA, S.M., Low-energy electron beam sterilization of solid alginate and chitosan, and their polyelectrolyte complexes, *Carbohydr. Polym.*, **261**, 2021, 117578, https://doi.org/10.1016/j.carbpol.2020.117578
15.MITTAL, H., RAY, S.S., KAITH, B.S., BHATIA, J.K., SHARMA, J., ALHASSAN, S.M., Recent progress in the structural modification of chitosan for applications in diversified biomedical fields, *European Polymer* Journal, **109**, 2018, 402–434, https://doi.org/10.1016/j.eurpolymj.2018.10.013
16. KIM, H.L., JUNG, G.Y., YOON, J.H., HAN, J.S., PARK, Y.J., KIM, D.G., ZHANG, M., KIM, D.J., Preparation and characterization of nano-sized hydroxyapatite/alginate/chitosan composite scaffolds for bone tissue engineering, *Mater. Sci. Eng. C*, **54**, 2015, 20–25, https://doi.org/10.1016/j.msec.2015.04.033
17.NIKPOUR, M.R., RABIEE, S.M., JAHANSHAHI, M., Synthesis and characterization of hydroxy-apatite/chitosan nanocomposite materials for medical engineering applications, *Compos. Part B Eng.*, **43**, 2012, 1881–1886, https://doi.org/10.1016/j.compositesb.2012.01.056
18.TSIOURVAS, D., SAPALIDIS, A., PAPADOPOULOS, T., Hydroxyapatite/chitosan-based porous three-dimensional scaffolds with complex geometries, *Mater. Today Commun.*, **7**, 2016, 59–66, https://doi.org/10.1016/j.mtcomm.2016.03.006

19.SINUSAITE, L., ANTUZEVICS, A., POPOV, A.I., ROGULIS, U., MISEVICIUS, M., KATELNIKOVAS, A., KAREIVA, A., ZARKOV, A., Synthesis and luminescent properties of Mn-doped alpha-tricalcium phosphate, *Ceram. Int.*, **47**, 2021, 5335–5340, https://doi.org/10.1016/j.ceramint.2020.10.114
20. XU, S., LIU, J., ZHANG, L., YANG, F., TANG, P., WU, D., Effects of HAp and TCP in constructing tissue engineering scaffolds for bone repair, *J. Mater. Chem. B*, **5**, 2017, 6110–6118, https://doi.org/10.1039/c7tb00790f
21. KATO, E., LEMLER, J., SAKURAI, K., YAMADA, M., Biodegradation property of beta-tricalcium phosphate-collagen composite in accordance with bone formation: A comparative study with bio-oss collagen® in a rat critical-size defect model, *Clin. Implant Dent. Relat. Res.*, **16**, 2014, 202–211, https://doi.org/10.1111/j.1708-8208.2012.00467.x
22. MAHMOUD, E.M., SAYED, M., EL-KADY, A.M., ELSAYED, H., NAGA, S.M., In vitro and in vivo study of naturally derived alginate/hydroxyapatite bio composite scaffolds, *Int. J. Biol. Macromol.*, **165**, 1346–1360, https://doi.org/10.1016/j.ijbiomac.2020.10.014
23. KANG, M.H., JANG, T.S., JUNG, H.D.O, KIM, S.M., KIM, H.E., KOH, Y.H., SONG, J., Poly(ether imide)-silica hybrid coatings for tunable corrosion behavior and improved biocompatibility of magnesium implants, *Biomed. Mater.*, **11**, 2016, doi: 10.1088/1748-6041/11/3/035003
24. CARFÌ PAVIA, F., CONOSCENTI, G., GRECO, S., LA CARRUBBA, V., GHERSI, G., BRUCATO, V., Preparation, characterization and in vitro test of composites poly-lactic acid/hydroxyapatite scaffolds for bone tissue engineering, *Int. J. Biol. Macromol.*, **119**, 2018, 945–953, https://doi.org/10.1016/j.ijbiomac.2018.08.007
25. SUGHANTHY, S.A.P., ANSARI, M.N.M., ATIQAH, A., Dynamic mechanical analysis of polyethylene terephthalate/hydroxyapatite biocomposites for tissue engineering applications, *J. Mater. Res. Technol.*, **9**, 2020, 2350-2356, https://doi.org/10.1016/j.jmrt.2019.12.066
26. HUANG, C., FANG, G., ZHAO, Y., BHAGIA, S., MENG, X., YONG, Q., RAGAUSKAS, A.J., Bio-inspired nanocomposite by layer-by-layer coating of chitosan/hyaluronic acid multilayers on a hard nano-cellulose-hydroxyapatite matrix, *Carbohydr. Polym.*, **222**, 2019, 115036, https://doi.org/10.1016/j.carbpol.2019.115036
27.GOLAN, O., SHALOM, H., KAPLAN-ASHIRI, I., COHEN, S.R., FELDMAN, Y., PINKAS, I., ALMOG, R.O., ZAK, A., TENNE, R., Poly(L-lactic acid) reinforced with hydroxyapatite and tungsten disulfide nanotubes, *Polymers (Basel)*, **13**, 2021, 1–20, https://doi.org/10.3390/polym13213851
28. GHOSH, R., SARKAR, R., Synthesis and characterization of sintered hydroxyapatite: a comparative study on the effect of preparation route, *J. Aust. Ceram. Soc.*, **54**, 2018, 71–80, https://doi.org/10.1007/s41779-017-0128-5
29.LI, Y., ZHANG, Z., ZHANG, Z., Porous Chitosan/Nano-Hydroxyapatite Composite Scaffolds Incorporating Simvastatin-Loaded PLGA Microspheres for Bone Repair, *Cells Tissues Organs*, **205**, 2018, 20–31, https://doi.org/10.1159/000485502
30. BOLLINO, F., ARMENIA, E., TRANQUILLO, E., Zirconia/hydroxyapatite composites synthesized via sol-gel: Influence of hydroxyapatite content and heating on their biological properties, *Materials (Basel)*, **10**, 757, https://doi.org/10.3390/ma10070757
31.GUESMI, Y., AGOUGUI, H., LAFI, R., JABLI, M., HAFIANE, A., Synthesis of hydroxyapatite-sodium alginate via a co-precipitation technique for efficient adsorption of Methylene Blue dye, *J. Mol. Liq.*, **249**, 2018, 912–920, https://doi.org/10.1016/J.MOLLIQ.2017.11.113
32. KWON, S.H., JUN, Y.K., HONG, S.H., KIM, H.E., Synthesis and dissolution behavior of β-TCP and HA/β-TCP composite powders, *J. Eur. Ceram. Soc.*, **23**, 2003, 1039–1045, https://doi.org/10.1016/S0955-2219(02)00263-7
33.SCALERA, F., GERVASO, F., SANOSH, K.P., SANNINO, A., LICCIULLI, A., Influence of the calcination temperature on morphological and mechanical properties of highly porous hydroxyapatite scaffolds, *Ceram. Int.*, **39**, 2013, 4839–4846, https://doi.org/10.1016/J.CERAMINT.2012.11.076

34. SALIMI, M.N., BRIDSON, R.H., GROVER, L.M., LEEKE, G.A., Effect of processing conditions on the formation of hydroxyapatite nanoparticles, *Powder Technol.*, **218**, 2012, 109–118, https://doi.org/10.1016/J.POWTEC.2011.11.049
35.DA SILVA FERNANDES, R., DE MOURA, M.R., GLENN, G.M., AOUADA, F.A., Thermal, microstructural, and spectroscopic analysis of Ca^{2+} alginate/clay nanocomposite hydrogel beads, *J. Mol. Liq.*, **265**, 2018, 327–336, https://doi.org/10.1016/j.molliq.2018.06.005
36. HUA, S., MA, H., LI, X., YANG, H., WANG, A., pH-sensitive sodium alginate/poly(vinyl alcohol) hydrogel beads prepared by combined Ca^{2+} crosslinking and freeze-thawing cycles for controlled release of diclofenac sodium, *Int. J. Biol. Macromol.*, **46**, 2010, 517–523, https://doi.org/10.1016/j.ijbiomac.2010.03.004
37.SAARAI, A., KASPARKOVA, V., SEDLACEK, T., SAHA, P., On the development and characterisation of crosslinked sodium alginate/gelatine hydrogels, *J. Mech. Behav. Biomed. Mater.*, **18**, 2013, 152–166, https://doi.org/10.1016/J.JMBBM.2012.11.010
38. LUO, H., ZUO, G., XIONG, G., LI, C., WU, C., WAN, Y., Porous nanoplate-like hydroxyapatite–sodium alginate nanocomposite scaffolds for potential bone tissue engineering, *Mater. Technol.*, **32**, 2017, 78–84, https://doi.org/10.1080/10667857.2015.1125045
39.LIU, D., LIU, Z., ZOU, J., LI, L., SUI, X., WANG, B., YANG, N., WANG, B., Synthesis and Characterization of a Hydroxyapatite-Sodium Alginate-Chitosan Scaffold for Bone Regeneration, *Frontiers in Materials*, **8**, 2021, https://doi.org/10.3389/fmats.2021.648980
40.JIN, H.H., KIM, D.H., KIM, T.W., SHIN, K.K., JUNG, J.S., PARK, H.C., YOON, S.Y., In vivo evaluation of porous hydroxyapatite/chitosan-alginate composite scaffolds for bone tissue engineering, *Int. J. Biol. Macromol.*, **51**, 2012, 1079–1085, https://doi.org/10.1016/J.IJBIOMAC.2012.08.027
41.BRENNAN, C.M., EICHHOLZ, K.F., HOEY, D.A., The effect of pore size within fibrous scaffolds fabricated using melt electrowriting on human bone marrow stem cell osteogenesis, *Biomed. Mater.*, **14**, 2019 , https://doi.org/10.1088/1748-605X/ab49f2
42.PITULICE, L., ISVORAN, A., CRAESCU, C.T., CHIRIAC, A., Scaling properties of the radius of gyration and surface area for EF-hand calcium binding proteins, *Chaos, Solitons & Fractals*, **40**, 684–690, https://doi.org/10.1016/J.CHAOS.2007.08.016
43.UNABIA, R., PIAGOLA, J.C., GUERRERO, J.R., VEQUIZO, R., GAMBE, J., ODARVE, M.K., SAMBO, B.R., Synthesis and characterization of nanocrystalline hydroxyapatite and biphasic calcium phosphate using $Ca(OH)_2$ and $(NH_4)H_2PO_4$, *Phys. Status Solidi Curr. Top. Solid State Phys.*, **12**, 2015, 572–575, https://doi.org/10.1002/PSSC.201400319
44.CARRODEGUAS, R.G., DE AZA, S., α-Tricalcium phosphate: Synthesis, properties and biomedical applications, *Acta Biomater.*, **7**, 2011, 3536–3546, https://doi.org/10.1016/J.ACTBIO.2011.06.019
45.JUN, Y.K., HONG, S.H., KONG, Y.M., Effect of Co-Precipitation on the Low-Temperature Sintering of Biphasic Calcium Phosphate, 2006 *J. Am. Ceram. Soc.*, **89**, 2016, 2295–2297, https://doi.org/10.1111/J.1551-2916.2006.00977.X
46.MOHAMMADI, Z., SHEIKH-MEHDI MESGAR, A., RASOULI-DISFANI, F., Preparation and characterization of single phase, biphasic and triphasic calcium phosphate whisker-like fibers by homogenous precipitation using urea, *Ceram. Int.*, **42**, 2016, 6955–6961. https://doi.org/10.1016/J.CERAMINT.2016.01.081

Manuscript received: 12.12.2023